Long-term variation of driven and unloading effects on polar cap dynamics

Ye Gao,[1,2] Margaret G. Kivelson,[1,2,3] Raymond J. Walker,[1,2] and James M. Weygand[2]

Received 8 September 2011; revised 8 December 2011; accepted 8 December 2011; published 4 February 2012.

[1] The influence of the solar wind on the magnetosphere-ionosphere system can be described in terms of driven and unloading processes. In a driven process, the response is proportional to the input with at most a small time delay. In an unloading process, the input energy accumulates without a corresponding output until, after a significant time delay, the energy is unloaded. The polar cap index, which has been used as a monitor of the polar cap activity, can be decomposed into a driven component and an unloading component through a linear regression with the polar cap index as response and $E_{K\text{-}R}$, an electric field proposed by Kivelson and Ridley (2008) as representative of the electric field imposed on the ionosphere by magnetopause reconnection when saturation is taken into account, and AL index as predictors. Such an analysis has been systematically applied day-by-day to most of the days in solar cycle 23. The driven-to-unloading ratio (*DUR*) is characterized in terms of the ratio of the regression coefficients for an appropriately normalized representation of the predictors. We have found that the ratio of the responses of the driven component to the unloading component is smaller near solar maximum than near solar minimum with variation of around ±5%. There is also a strong annual variation of as much as ±15% with stronger driven-to-unloading ratio in summer than in winter. The variation of driven-to-unloading ratio in solar cycle 23 is explained in terms of enhancement of ionospheric conductance by electron precipitation during strong solar wind high-speed streams and the annual variation can be understood as seasonal variation of conductance caused by solar illumination.

Citation: Gao, Y., M. G. Kivelson, R. J. Walker, and J. M. Weygand (2012), Long-term variation of driven and unloading effects on polar cap dynamics, *J. Geophys. Res.*, *117*, A02203, doi:10.1029/2011JA017149.

1. Introduction

[2] *Troshichev et al.* [1988] defined the polar cap (PC) index, PCN for the northern hemisphere and PCS for the southern hemisphere, as an instantaneous monitor of geomagnetic activity over the polar cap directly driven through the coupling between the solar wind and the magnetosphere-ionosphere system. Its definition is based on a statistical linear relationship between the merging electric field of the solar wind (E_m) [*Kan and Lee*, 1979] and the projected local magnetic field perturbations (ΔF_{PROJ}) at a high-latitude station (assumed to be in the polar cap) on the Earth's surface,

$$\Delta F_{PROJ} = \beta_0 + \beta_1 E_m, \tag{1}$$

where β_0 is the intercept and β_1 is the regression coefficient. Qaanaaq (86.5° magnetic latitude) is used to characterize ΔF_{PROJ} in the northern hemisphere and Vostok (−83.6° magnetic latitude) is used in the southern hemisphere. In equation (1), E_m is calculated from the solar wind bulk velocity $\boldsymbol{u}$, and magnetic field $\boldsymbol{B}$ through

$$E_m = uB_{yz}\sin^2\theta/2, \tag{2}$$

where u is the magnitude of the solar wind velocity, $B_{yz} = (B_y^2 + B_z^2)^{1/2}$ in the geocentric solar magnetic (GSM) coordinate system, and θ is the solar wind clock angle measured from the GSM z axis [*Kan and Lee*, 1979]. The local magnetic field perturbation is projected to the "optimum direction" perpendicular to the mean transpolar DP2 (polar disturbance of the second type) current to get ΔF_{PROJ}, which is calculated as

$$\Delta F_{PROJ} = \Delta H \sin\gamma + \Delta D \cos\gamma, \tag{3}$$

where $\gamma = \lambda \pm D_E + \varphi + UT\cdot 15°$, ΔH and ΔD are magnetic field deviations from a pre-established quiet level (For PCN, the reference is the internal field. For PCS, the reference is the sum of the internal field and the QDC (quiet day curve) [*Janzhura and Troshichev*, 2008]), D_E is the station's average declination angle, λ is its geographical longitude, and φ, called the optimum direction angle, is in principle, the UT-dependent angle between the average DP2 current and the

[1]Department of Earth and Space Sciences, University of California, Los Angeles, California, USA.
[2]Institute of Geophysics and Planetary Physics, University of California, Los Angeles, California, USA.
[3]Department of Atmospheric, Oceanic and Space Sciences, University of Michigan, Ann Arbor, Michigan, USA.

0148-0227/12/2011JA017149

noon-midnight meridian [*Troshichev et al.*, 1988; *Stauning*, 2011]. Then the PC index is calculated as

$$\mathrm{PC} = (\Delta F_{\mathrm{PROJ}} - \beta_0)/\beta_1\eta, \tag{4}$$

where η = 1 mV/m is introduced to make the PC index dimensionless. The PC index is used to measure the strength of the direct driving of the magnetosphere from the solar wind. See *Stauning* [2011] for a detailed discussion of the derivation of the PC index.

[3] Previous studies have demonstrated that the PC index can be used to monitor various ionospheric quantities, e.g., the cross polar cap potential [*Troshichev et al.*, 1996; *Ridley and Kihn*, 2004], cross polar cap electric field and velocity [*Troshichev et al.*, 2000; *Fiori et al.*, 2009], auroral power [*Liou et al.*, 2003], and hemispheric Joule heating production rate [*Chun et al.*, 1999, 2002].

[4] Other than the PC index, three techniques are commonly used to quantify the state of the polar ionosphere: the Assimilative Mapping of Ionospheric Electrodynamics (AMIE), which models the ionosphere currents, and thus, infers electric fields from ground magnetometer measurements [e.g., *Ridley and Kihn*, 2004]; the Defense Meteorological Satellite Program (DMSP), which performs in situ observations of plasma drift velocity using low-altitude satellites [e.g., *Hairston et al.*, 1998]; and the Super Dual Auroral Radar Network (SuperDARN), which infers the plasma velocity from radar measurements [e.g., *Ruohoniemi and Baker*, 1998]. All three techniques contribute in an important way to studies of ionosphere physics, and yet all three (as well as the PC index) have limitations. For most intervals, the alternative techniques give similar results. However, temporal continuity is critical for a statistical study of the response of the polar ionosphere to solar wind driving and the magnetospheric dynamics, so we required an index for which records are nearly continuous in time. The PC index satisfies this requirement and, in contrast with the AMIE technique, is based on a simple magnetic measurement. For these reasons, we have elected to use the PC index to characterize the electric field in the polar cap.

[5] In exploring the physical mechanism of the saturation of the cross polar cap potential (CPCP), *Kivelson and Ridley* [2008] argued that part of the merging electric field is reflected at the top of the ionosphere and a modified form ($E_{\mathrm{K\text{-}R}}$), designated as the Kivelson-Ridley electric field, represents better the field actually imposed on the ionosphere. Although different models have been proposed to explain saturation of the CPCP [e.g., *Siscoe et al.*, 2002, 2004; *Borovsky et al.*, 2009], they all predict electric fields similar to that of *Kivelson and Ridley* [2008]. Thus, in this study, we take $E_{\mathrm{K\text{-}R}}$ as representative of the electric field imposed on the polar ionosphere by magnetopause reconnection in a form that takes saturation into account. With this expectation, a modified electric field

$$E_{\mathrm{K-R}} = E_{\mathrm{m}} 2\Sigma_{\mathrm{A}}/(\Sigma_{\mathrm{P}} + \Sigma_{\mathrm{A}}), \tag{5}$$

should be used instead of E_{m}. Here $2\Sigma_{\mathrm{A}}/(\Sigma_{\mathrm{P}}+\Sigma_{\mathrm{A}})$ is the transmission coefficient. In equation (5), Σ_{P} is the Pedersen conductance, fixed at 10S [*Kivelson and Ridley*, 2008; Y. Gao et al., Utilizing the polar cap index to explore strong driving of polar cap dynamics, submitted to *Journal of Geophysical Research*, 2011]. Σ_{A}, the Alfvén conductance of the Alfvén wing, is calculated as

$$\Sigma_{\mathrm{A}} = 1/\mu_0 v_{\mathrm{A}}, \tag{6}$$

where $\mu_0 = 4\pi \times 10^{-7}$ H/m and the Alfvén velocity in the solar wind, $v_{\mathrm{A}} = B/(\mu_0\rho_{\mathrm{sw}})^{1/2}$, is computed by using the solar wind magnetic field magnitude B and density ρ_{sw}. A corrected form that takes into account the density variation from the solar wind to the polar cap would replace equation (6) by

$$\Sigma_{\mathrm{A}} = \left(\rho_{\mathrm{pc}}/\rho_{\mathrm{sw}}\right)^{1/4}(1/\mu_0 v_{\mathrm{A}}), \tag{7}$$

where ρ_{pc} is the mass density in the low-altitude polar cap (e.g., $2R_{\mathrm{E}}$ from the center of Earth) at the top of the ionosphere. Since the values of ρ_{pc} are not routinely measured and the probable values of $(\rho_{\mathrm{pc}}/\rho_{\mathrm{sw}})^{1/4}$ are likely to differ from 1 by no more than a factor of 2 (see the appendix of *Kivelson and Ridley* [2008]), equation (6) is used with the understanding that this introduces errors but no more than a few tens of percent. Under nominal solar wind conditions, Σ_{A} is close to Σ_{P}. Consequently, $E_{\mathrm{K\text{-}R}} \approx E_{\mathrm{m}}$. When the solar wind driving gets stronger, especially when $E_{\mathrm{m}} > 10$mV/m, Σ_{A} becomes smaller than Σ_{P}, and thus $E_{\mathrm{K\text{-}R}} < E_{\mathrm{m}}$. The concept of $E_{\mathrm{K\text{-}R}}$ has been very successful in explaining the cross polar cap potential saturation [*Kivelson and Ridley*, 2008; *Borovsky et al.*, 2009]. Y. Gao et al. (submitted manuscript, 2011) compared the consistency between PCN and E_{m} and between PCN and $E_{\mathrm{K\text{-}R}}$ for 53 one to two day intervals with subintervals during which $E_{\mathrm{m}} > 10$ mV/m and typically PCN > 5 from 1998 to 2006. They found that PCN generally correlates with $E_{\mathrm{K\text{-}R}}$ better than with E_{m}, especially when $E_{\mathrm{K\text{-}R}}$ is significantly different from E_{m}.

[6] In studying magnetospheric substorms, *Akasofu* [1979] characterized the response, which is usually represented by geomagnetic indices, e.g., AE, AL or the PC index, of the magnetosphere-ionosphere system to the solar wind input, e.g., the coupling function between the solar wind and the magnetosphere-ionosphere system, in terms of driven processes and unloading processes. A driven process is one for which the response is virtually identical with the input, or perhaps with at most a small time delay. In contrast, an unloading process is one in which the input is integrated over time without a corresponding output, until after a long time delay the energy is unloaded. This process is internal to the magnetosphere-ionosphere system, and hence the response bears little resemblance to the input [*McPherron and Baker*, 1993]. *Bargatze et al.* [1985] confirmed this argument using AL as the response and uB_{s} as input. In this formula, u is the solar wind bulk speed, and $B_{\mathrm{s}} = |B_{\mathrm{z}}|$, for $B_{\mathrm{z}} < 0$ and $B_{\mathrm{s}} = 0$, for $B_{\mathrm{z}} \geq 0$, where the interplanetary magnetic field (IMF) is expressed in geocentric solar magnetospheric (GSM) coordinates. Gao et al. (submitted manuscript, 2011) separated the driven component and the unloading component of AL by calculating the regression of AL on $E_{\mathrm{K\text{-}R}}$, i.e., $\mathrm{AL_D} = \beta_0 + \beta_1 E_{\mathrm{K\text{-}R}}$, and identifying the residuals, $\mathrm{AL_U} = \mathrm{AL} - \mathrm{AL_D}$, as the unloading component. Gao et al. (submitted manuscript, 2011) also found that $\mathrm{AL_U}$ correlates quite well with the PC index. A linear regression

with PCN as response and $E_{K\text{-}R}$ and AL_U as predictors is given by

$$PCN = \alpha_0 + \alpha_1 E_{K-R} + \alpha_2 AL_U + \varepsilon, \quad (8)$$

where α_0 is intercept, and α_1 and α_2 are regression coefficients; ε, often assumed to be the error with zero expectation and constant variance [*Myers*, 2000], represents the influence from noise and potential unidentified processes influencing PCN (e.g., viscous interaction between the solar wind and the Earth's magnetosphere at the low-latitude boundary layer [*Axford*, 1964]). In equation (8), $E_{K\text{-}R}$ represents the driving contribution to the PC index on flux tubes linked to the solar wind by dayside reconnection [*Kivelson and Ridley*, 2008], and AL_U measures the unloading contribution primarily caused by nightside energy release [*McPherron and Baker*, 1993]. To quantify the contributions from $E_{K\text{-}R}$ and AL_U, standardization procedures are applied to both $E_{K\text{-}R}$ and AL_U by calculating normalized quantities referred to as their z-scores (zs) [*Myers*, 2000] and defined as

$$Z = (X - \mu_X)/\sigma_X, \quad (9)$$

where X is any variable with expectation μ_X and standard deviation σ_X. Thus, equation (8) is modified to

$$PCN = \beta_0 + \beta_1\, zs(E_{K-R}) + \beta_2\, zs(AL_U) + \varepsilon, \quad (10)$$

where β_0 is the intercept, and β_1, β_2 are regression coefficients. ε is the same as in equation (8). Then the relative importance of $E_{K\text{-}R}$ and AL_U in determining PCN is measured by the relative magnitudes of β_1, β_2 (Gao et al., submitted manuscript, 2011).

[7] In this study, we investigate the driven and unloading contributions to the PC index by extending the work of Gao et al. (submitted manuscript, 2011) to encompass solar cycle 23. In section 2, we describe the data used. In section 3, we apply regression analysis day-by-day from 1 February 1998 to 31 December 2009. We find that (1) the unloading contribution to the PC index is confirmed; (2) the relative contributions of driven and unloading components varies within solar cycle 23 with a magnitude $\pm$ 5%, with the driven-to-unloading ratio highest near solar minimum and lowest after solar maximum; (3) the driven-to-unloading ratio peaks in summer and decreases in winter; and (4) the magnitude of the annual variation can be as large as $\pm$ 15%. Finally, in section 4, we summarize the results and discuss the physical mechanisms that can be responsible for the variation within a solar cycle and annual variation.

2. Data

[8] In this study, we use the 1 min resolution PC index from the northern hemisphere (PCN) since it is more frequently available. PCS, when it is available, is also used but only to confirm the values of PCN. The data used in this paper were acquired between 1 February 1998 and 31 December 2006. Different definitions of these indices have been used since they were introduced in 1988 [*Troshichev et al.*, 1988; *Vennerstrøm*, 1991; *Troshichev et al.*, 2006]. We have used the PCN index recorded by the Qaanaaq station (86.5° magnetic latitude) and produced by the Danish National Space Institute (DTU space); the PCS index in this paper is from Vostok (−83.4° magnetic latitude) and is produced by the Arctic and Antarctic Research Institute [*Troshichev and Lukianova*, 2002].

[9] The solar wind properties are monitored by the ACE (Advanced Composition Explorer) spacecraft. ACE was launched on 25 August 1997 to Lagrange Point 1 to monitor the solar wind. We use 1 min resolution magnetic field vectors and plasma moments provided by the Magnetic Field (MAG) [*Smith et al.*, 1998] and Solar Wind Electron, Proton, and Alpha Monitor (SWEPAM) [*McComas et al.*, 1998] instruments. The GSM coordinate system is adopted for analyzing vectors. The solar wind data have been propagated to $X_{GSM} = 17R_E$ using the *Weimer et al.* [2003] technique.

[10] The AE index, obtained from the World Data Center in Kyoto, comes from the geomagnetic variations in the horizontal component observed at 12 selected observatories near the auroral zone in the northern hemisphere. The data from these stations are superposed as a function of UT. AU and AL form the upper envelope and lower envelope of the superposed traces, respectively. The difference, AU - AL, defines the AE index.

3. Analysis

[11] In this study, we apply the regression analysis day by day from 1 February 1998 to 31 December 2009. This includes most of solar cycle 23. Here, the contributions from $E_{K\text{-}R}$ and AL_U relative to the variations of PCN are of interest. The model that we used in this study is based on equation (10) and rewritten as

$$PCN = \beta_0 + \beta_1\, zs(E_{K-R}) + \beta_2\, zs(AL_U) + \varepsilon, \quad (11)$$

where β_0 is the intercept and β_1, β_2 are the regression coefficients between PCN and $zs(E_{K\text{-}R})$ and between PCN and $zs(AL_U)$ [*Myers*, 2000; Gao et al., submitted manuscript, 2011]. The consistency between the measured PCN and the regressed PCN is quantified by R^2 and the error variance. R^2, also called the coefficient of determination [*Myers*, 2000], is defined as

$$R^2 = 1 - SS_{Res}/SS_{Total}. \quad (12)$$

[12] In the above equation, SS_{Res} is the residual sum of squares, calculated as

$$SS_{Res} = \|\boldsymbol{y} - \hat{\boldsymbol{y}}\|^2, \quad (13)$$

where $\boldsymbol{y}$ is the vector of observations and $\hat{\boldsymbol{y}}$ is the vector of least square fits. Here $||\boldsymbol{x}||$ indicates the Euclidean norm of a vector $\boldsymbol{x}$. SS_{Total}, the total sum of squares, is defined as

$$SS_{Total} = \|\boldsymbol{y} - \bar{y}\mathbf{1}\|^2, \quad (14)$$

where $\bar{y}$ is the sample mean and $\mathbf{1}$ is given by $\mathbf{1} = (1, 1, \cdots, 1)^T$. R^2, which takes values between 0 and 1, represents the proportion of variation in the response data that is explained by the model [*Myers*, 2000]. The error variance, an estimate of var(ε), is estimated as

$$\sigma^2 = SS_{Res}/(n - p), \quad (15)$$

where n is the number of observations and p is the number of parameters, e.g., $p = 3$ for equation (11).

[13] The distribution of R^2 for all the cases from 1 February 1998 to 31 December 2009 is shown in Figure 1. The

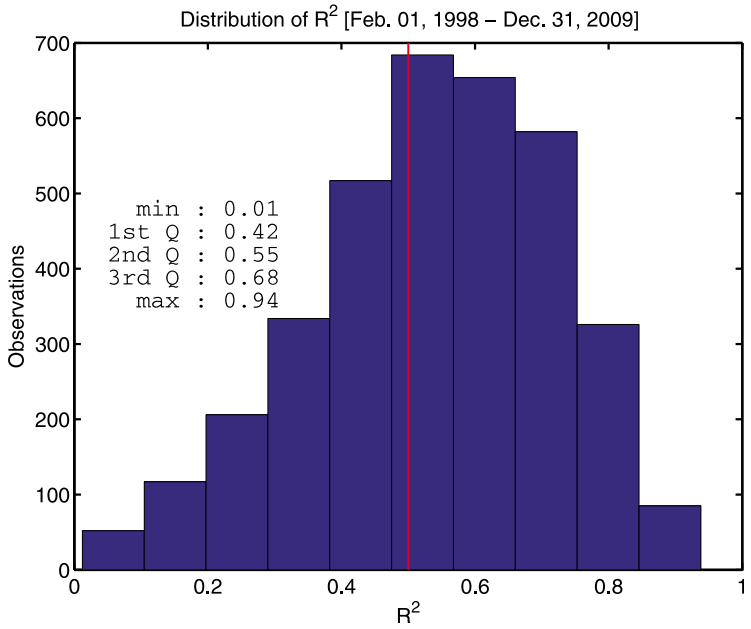

Figure 1. Distribution of R^2 when applying equation (11) to cases between 1 February 1998 and 31 December 2009. $R^2 = 0.5$, shown as the red vertical line, has been used as a criterion to select events for further analysis. Here 2155 out of 3557 cases satisfies this criterion.

distribution of R^2 can be summarized as: minimum: 0.01; first quartile: 0.42; median: 0.55; third quartile: 0.68; and maximum: 0.94. $R^2 \geq 0.5$ is used as a criterion to select cases for further analysis. 2155 out of 3557 cases are retained. (Owing to missing data, not every day returns a result.) Among those cases with R^2 less than 0.5, some are influenced by unusual activity, (Gao et al., submitted manuscript, 2011, Figure 18), but most are because the PCN signal-to-noise ratio is too small to be distinguished from background noise. An example of such a case is shown in Figure 2. For this interval, PCN is small (PCN < 1.8). The blue line is the measured PCN index, while the green line represents the PCN index predicted from equation (11). Clearly, they are inconsistent. This is confirmed by the low R^2 (0.37). In contrast, Figure 3 shows a case on 20 November 2003. This is an interval when the magnetosphere-ionosphere system is experiencing strong driving from the solar wind. The measured PCN is roughly an order of magnitude larger than for

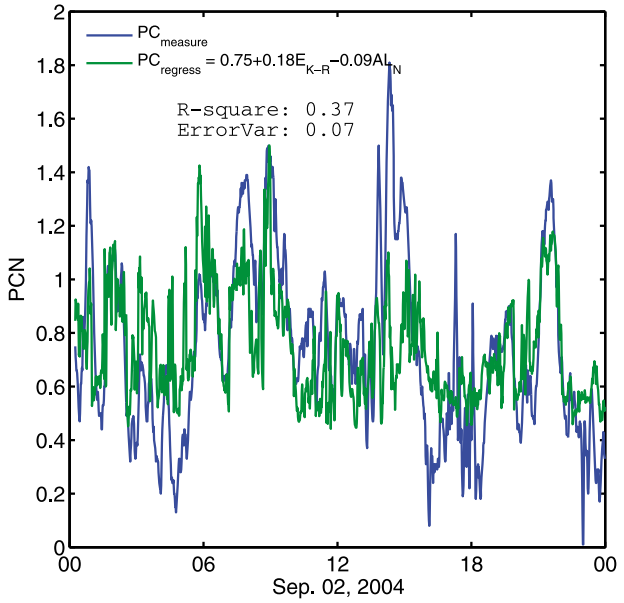

Figure 2. Comparison between the PC index and the predicted PC index based on solar wind parameters for 2 September 2004. The blue line is the measured PCN index. The green is the predicted PCN index based on a linear regression from Kivelson-Ridley electric field ($E_{K\text{-}R}$) and unloading component of AL (AL_U).

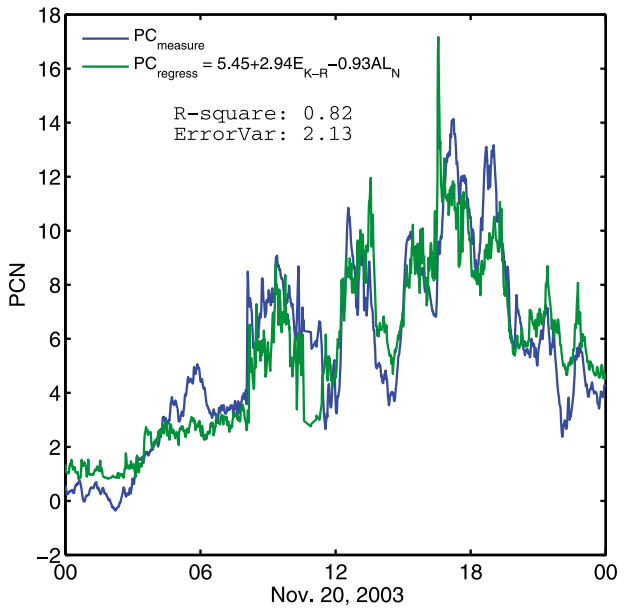

Figure 3. As for Figure 2 for a different event on 20 November 2003.

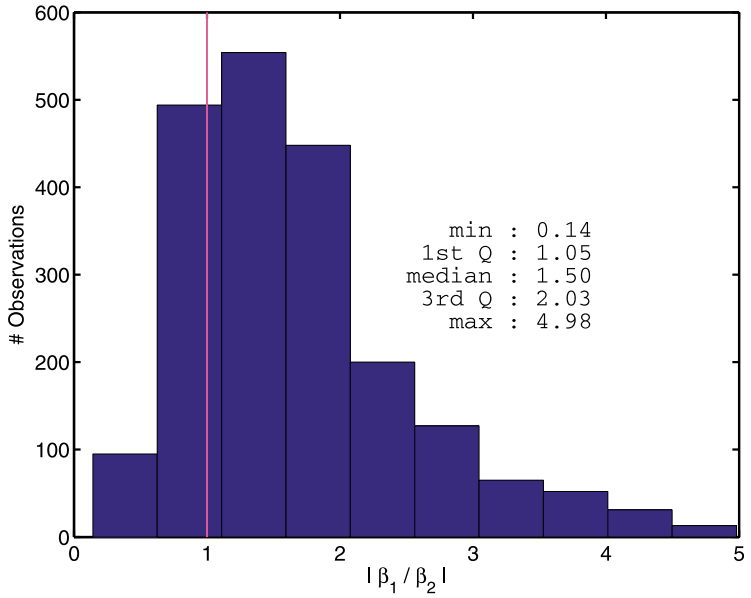

Figure 4. Histogram of *DUR* for events with $R^2 \geq 0.5$ between 1 February 1998 and 31 December 2009, which can be summarized as: minimum: 0.14; first quartile: 1.05; median: 1.5; third quartile: 2.03; maximum: 4.98. The red vertical line indicates equal contributions from driven and unloading to PCN.

the case of Figure 2, and the measured and predicted PCN are highly correlated. For this case, R^2 is 0.83.

[14] To describe the relative importance of the driven and unloading effects on the PC index, we define the driven-to-unloading ratio (*DUR*) as

$$DUR = |\beta_1/\beta_2|, \tag{16}$$

where β_1 and β_2 are regression coefficients in equation (11). The distribution of *DUR* is shown in Figure 4. Probability concentrates between 0.5 and 3 with summary statistics: minimum: 0.14; first quartile: 1.05; median: 1.50; third quartile: 2.03; and maximum 4.98.

3.1. Variation in Solar Cycle 23

[15] The time series with 1 day resolution of *DUR* from 1 February 1998 to 31 December 2009 is shown in Figure 5. Large variation characterizes the evolution of *DUR* through solar cycle 23. To obtain more useful

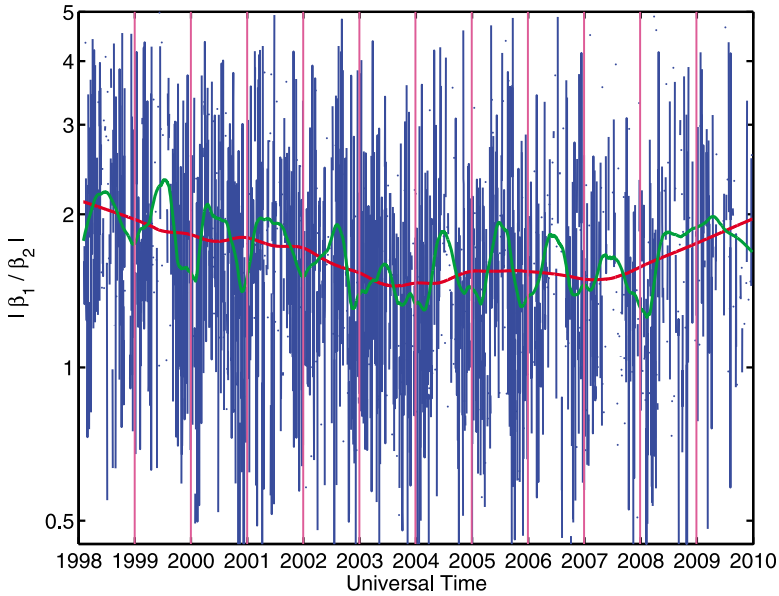

Figure 5. The time series with 1 day resolution of *DUR* from 1 February 1998 to 31 December 2010 is plotted in blue. The green line is the LOWESS smoothed blue line with $k = 60$ (described in text). The red line is the LOWESS smoothed blue line with $k = 700$. The magenta vertical lines separate different years. Notice that the y axis is spaced in a log scale.

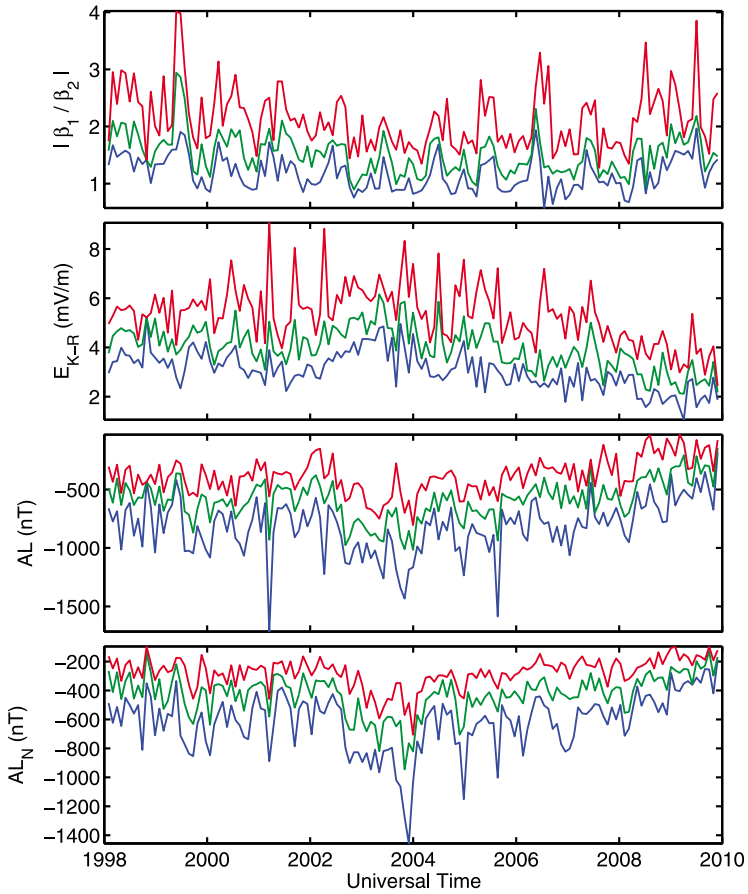

Figure 6. Time series of the monthly averaged quantities from top to bottom: *DUR*, $E_{K\text{-}R}$, AL, and AL_U. The red, green and blue lines indicate the third quartile, median and first quartile, respectively.

information, appropriate smoothing needs to be applied to the raw *DUR* time series. A popular choice is the locally weighted scatterplot smoother (LOWESS), which achieves smoothing by fitting simple models (e.g., linear or quadratic polynomials) to localized subsets of the data to build a function to identify the systematic part of the variation in the data [*Cleveland*, 1979]. For each point x_0, k nearest points, denoted by $N(x_0)$, are identified. $\Delta(x_0) = \max_N | x_0 - x_i |$, the distance of the furthest near-neighbor from x_0, is computed. Weights w_i are assigned to each point in $N(x_0)$, using the tri-cube weight function $W(| x_0 - x_i | / \Delta(x_0))$, where

$$W(u) = \left[\left(1-u^3\right)^3\right]_+. \tag{17}$$

Here $[x]_+ = x$, if $x > 0$, otherwise $[x]_+ = 0$. The predicted value at x_0 is fitted from the weighted least square confined to $N(x_0)$ using the weights computed above. k serves as the smoothing parameters, with smoother time series resulting from larger k.

[16] The raw and LOWESS smoothed *DUR*s are shown in Figure 5. The green line is the LOWESS smoothed *DUR* with $k = 60$ ($\sim \pm 1$ month), while the red line has $k = 700$ ($\sim \pm 1$ year). The green line reveals the annual variations of the *DUR* which peaks in summer and drops low in winter. This topic is pursued in section 3.2. The red line removes most of the annual variations and represents the variation of *DUR* within solar cycle 23. It reveals an interesting property. Within solar cycle 23, the *DUR* decreased as solar activity increased and increased as solar activity decreased. It is estimated that the solar cycle effect varies the trend of *DUR* by $\pm 5\%$.

[17] Quantities related to PCN are plotted in Figure 6. From top to bottom, plotted are the monthly averaged *DUR*, $E_{K\text{-}R}$, AL and AL_U. The blue, green and red lines are first quartile, median and third quartile, respectively. During the transition from solar minimum to solar maximum, the electric field increases as expected. Nevertheless, the magnitude of AL_U increases even more and thus reduces the *DUR*.

[18] We should also comment on the difficulty of characterizing the solar wind field imposed on the magnetosphere during solar maximum. At solar maximum, the amplitude of fluctuations in the solar wind increases and, for this reason, the propagation technique used to estimate the field at the magnetopause from the field at ACE is more likely to fail [*Ridley*, 2000; *Ashour-Abdalla et al.*, 2008]. However, we have compared the regression results with $E_{K\text{-}R}$ calculated from the propagated ACE data and that calculated from a near Earth satellite, e.g., Geotail, THEMIS, when it is in the solar wind near solar maximum and solar minimum. The results only differ mildly and no significant bias has been identified. Thus, even though the propagation uncertainty would contribute to the variation of *DUR*, we treat it as a secondary factor.

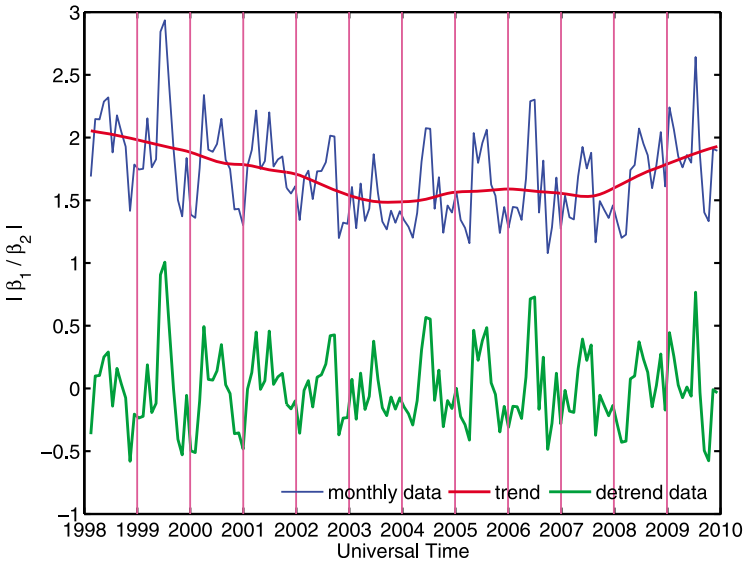

Figure 7. Monthly *DUR* in blue and its solar cycle trend in red. The green line is the detrended monthly *DUR*.

[19] We believe that the change of *DUR*, the relative contribution of $E_{K\text{-}R}$ and AL_U to PCN, through solar cycle 23 is likely to result from the enhancement of Hall conductance in the auroral zone induced by increased electron precipitation just after solar maximum, concurrent with the peak strength of high-speed streams [*Emery et al.*, 2009]. As we have mentioned earlier, the PC index depends on the strength of ionospheric Hall currents both in the polar cap [*Vennerstrøm et al.*, 1991; *Takalo and Timonen*, 1998] and in the auroral electrojet (Gao et al., submitted manuscript, 2011). The form of the dependence of the polar cap currents on $E_{K\text{-}R}$ is not likely to change much through a solar cycle. The Hall current, contributed by the solar wind driving, is calculated as

$$J_D = \Sigma_I E_{K\text{-}R}, \tag{18}$$

where J_D represents the Hall current driven by the solar wind electric field, and Σ_I is the Hall conductance that arises from ionization by solar illumination [e.g., *Robinson and Vondrak*, 1984]. The Hall current in the auroral zone is dominated by electron precipitation, implying that the current in the auroral electrojet, J_U, can be expressed as

$$J_U = \Sigma_{E\text{-}P} E_U, \tag{19}$$

where $\Sigma_{E\text{-}P}$ stands for the Hall conductance in the night hemisphere primarily caused by the electron precipitation (E-P) [e.g., *Spiro et al.*, 1982], and E_U is the ionospheric signature of the tail convection electric field. The unloading AL index, AL_U, primarily responds to J_U [*Bargatze et al.*, 1985; *McPherron and Baker*, 1993] and can be expressed as

$$AL_U \propto J_U = \Sigma_{E\text{-}P} E_U, \tag{20}$$

Østgaard et al. [2002] related AE and $\Sigma_{E\text{-}P}$ to P_e, the hemispherical energy dissipation by auroral electrons, as

$$\Sigma_{E\text{-}P} \propto P_e^{1/2}. \tag{21}$$

Emery et al. [2009] studied the relationship between the hourly averaged global energy dissipation by auroral electrons ($P_{e,G}$) and three types of solar wind structures: slow speed streams (v_{sw} < 400km/s), high-speed streams (HSS) (v_{sw} > 400km/s), and transient structures associated with coronal mass ejections (CME) over three solar cycles. Here $P_{e,G}$ measures the energy dissipation by auroral electrons in both hemispheres. Therefore, apart from seasonal variations, $P_{e,G}$ is approximately $2P_e$, i.e.,

$$P_{e,G} \approx 2P_e. \tag{22}$$

Emery et al. [2009] found that $P_{e,G}$, and thus P_e, is most effectively controlled by HSS whose strength peaks at the beginning of the descending phase of a solar cycle.

[20] If we assume that, on the time scale of months, the magnitudes of $E_{K\text{-}R}$ and E_U vary proportionally, i.e.,

$$E_U \propto E_{K\text{-}R}, \tag{23}$$

the relative magnitude of direct driving and unloading of the PC index in solar cycle 23 can be understood. An increase of $\Sigma_{E\text{-}P}$ due to the enhancement of P_e results in a decrease in *DUR*. As P_e, and thus $\Sigma_{E\text{-}P}$, peak slightly after the solar maximum, *DUR* reaches its minimum at that phase of the solar cycle. Thereafter, *DUR* starts to increase as P_e and $\Sigma_{E\text{-}P}$ decrease (see *Emery et al.* [2009, Figure 2c] for a detailed description of variation of P_e in solar cycle 23). However, at this stage, the proposed interpretation is speculative. Further studies of the variation with solar cycle of the relative importance of $E_{K\text{-}R}$ and AL_U in driving the PC index are needed.

3.2. Seasonal Variation

[21] The green line in Figure 5 shows that superimposed on the solar cycle variation of the *DUR* there is also an annual variation. Considerations related to the sources of conductance at high latitudes can also help explain the seasonal effects in *DUR*, the matter to which we turn in this

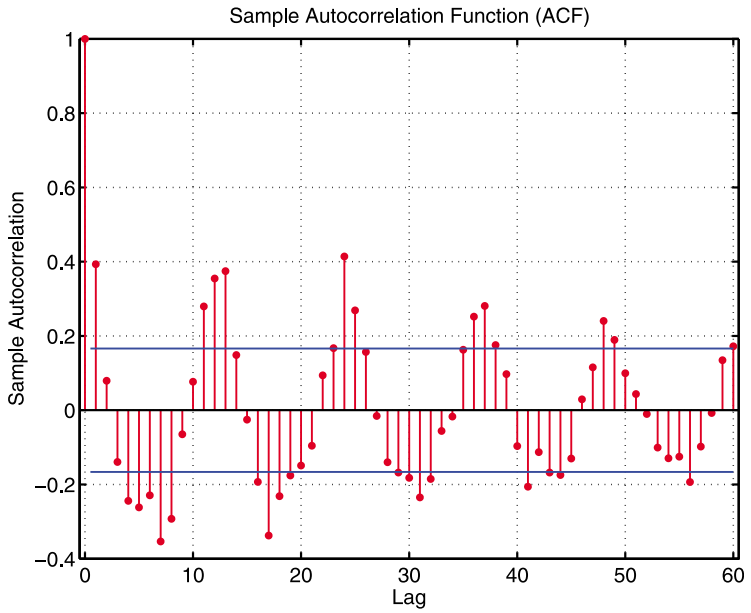

Figure 8. Autocorrelation function (ACF) of the detrended monthly *DUR* time series; 1 lag in the *x* axis indicates a month. Thus, with positive peaks at lags 13, 24, 37, 48, this indicates a periodicity of 12 months.

section. We calculated the monthly *DUR* by using 30 day block averages. As the solar cycle trend is independent of seasonal variations, we remove it as shown in Figure 7 by subtracting the trend (red line) from the monthly *DUR*. An autocorrelation function (ACF) [e.g., *Shumway and Stoffer*, 2006] of the detrended monthly *DUR* time series is shown in Figure 8. A periodicity of 12 months is identified with peaks at lags of 13, 24, 37, and 48 months in ACF. To better resolve the periodicity, spectral analysis is performed on the monthly detrended *DUR* time series. Figure 9 shows the periodogram [e.g., *Shumway and Stoffer*, 2006] of the detrended monthly *DUR* time series. The abscissa is physical frequency with units per month. The ordinate is power per frequency. The strongest power is peaked at 0.08/month corresponding to a 12 month periodicity. A smaller peak near 0.16/month corresponds to a semi-annual variation. Other small peaks remain.

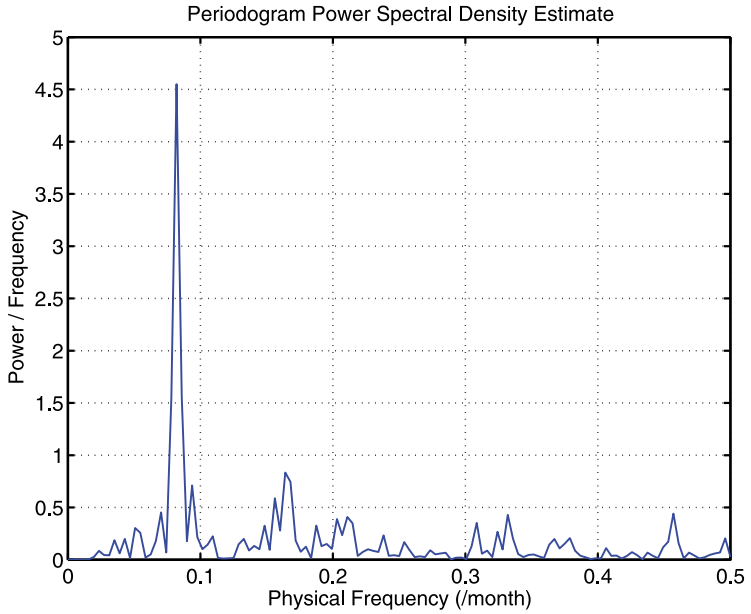

Figure 9. Periodogram of the detrended monthly *DUR* time series. The abscissa is physical frequency with unit per month. The ordinate is power per frequency. Strong power concentrates on 0.08/month, which corresponds to a 12 month period. Some power lies at 0.16/month, which maps to the semi-annual variation.

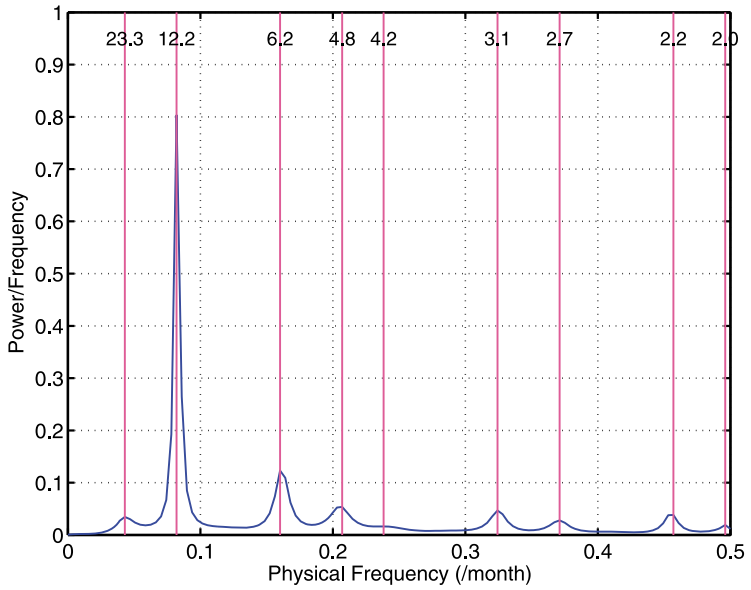

Figure 10. Spectrum estimated by using the Yule-Walker method (described in text). The format is the same as Figure 9. The vertical magenta lines locate the positions of the local peaks. The numbers are the periods in months corresponding to the peaks.

[22] A smoother spectral estimation is obtained through the Yule-Walker method [*Yule*, 1927; *Walker*, 1931]. In this method, an autoregressive model of order p (AR(p)) is fitted to the time series, as

$$x_t = \varphi_1 x_{t-1} + \varphi_2 x_{t-2} + \ldots + \varphi_p x_{t-p} + \omega_t,$$

where x_t is the observation at time t, and φ_1, φ_2, …, φ_p are regression coefficients, and ω_t are assumed to be Gaussian white noise with $E(\omega_t) = 0$ and $\text{var}(\omega_t) = \text{constant}$. The spectral estimation is calculated theoretically from φ_1, φ_2, …, φ_p [e.g., *Shumway and Stoffer*, 2006]. The optimal order p is evaluated by Akaike's information criterion [*Akaike*, 1973], defined as

$$\text{AIC} = \ln \sigma_m^2 + (n + 2p)/n. \quad (24)$$

Here

$$\sigma_m^2 = SS_{\text{Res}}/n, \quad (25)$$

where SS_{Res} is the residual sum of squares using autoregression of order p, n is the number of observations. AIC balances the goodness of fit, measured by σ_m^2, against the model complexity, quantified by p. An optimal model results in minimum AIC. The optimal order in our study is $p = 24$. The corresponding Yule-Walker spectrum is shown in Figure 10. The similarity between Figure 10 and Figure 9 is clear with major peaks aligning at the same physical frequencies. The advantage of the Yule-Walker spectrum is that only important peaks remain, which provides us a chance to study them one by one. For our spectrum, two peaks at 12.2 and 6.2 months are much more significant than the rest. Recall that the monthly *DUR* is calculated by running block average of 30 days. Thus, the peak at 12.2 months corresponds to $12.2 \times 30 \approx 365$ days, or the annual variation. Similarly, the peak at 6.2 months gives the semi-annual variation. We interpret the annual variation in terms of seasonal variations of ionospheric conductance. Conductance is enhanced in summer when the solar zenith angle decreases. For example, *Robinson and Vondrak* [1984] found that $\Sigma_1 \propto \cos^{1/2}\chi$, where χ is solar zenith angle. With higher Hall conductance in summer, a higher *DUR* in summer is expected. AL, on the other hand, arises from currents that flow in regions where the conductivity is dominated by electron precipitation [e.g., *Spiro et al.*, 1982].

[23] Previous studies have demonstrated that conductivity caused by electron precipitation varies with season. For example, *Ridley* [2007] proposed that there was 20% more electron precipitation in the winter hemisphere than in the summer hemisphere. *Emery et al.* [2008] found that the power in precipitated electrons was 35% higher in the summer hemisphere under quiet conditions and 40% higher in the winter hemisphere under active conditions. Thus, there is some ambiguity regarding the seasonal variation of precipitation-controlled conductivity, and it is beyond the scope of this paper to investigate this matter. Our results suggest that the seasonal variations of solar illumination outweigh the effects of electron precipitation in controlling the *DUR* as shown in Figure 5. In Figure 5, the green line, the LOWESS smoothed *DUR* with $k = 60$, peaks in summer every year, indicating that, in general, the driven component increases more than the unloading component in summer months. The current study is consistent with *Vennerstrøm et al.*, [1991] who showed that the PC index correlates better with the AE, and AL indices in winter ($R = 0.8$–0.9) than in summer ($R = 0.6$–0.8). In winter, smaller conductance resulting from diminished solar illumination results in weaker direct driving (compared with summer) of the PCN by the solar wind, without greatly affecting the unloading contributions. The consequence is that there will be higher correlations between the PC and AE, AL indices in winter than in summer.

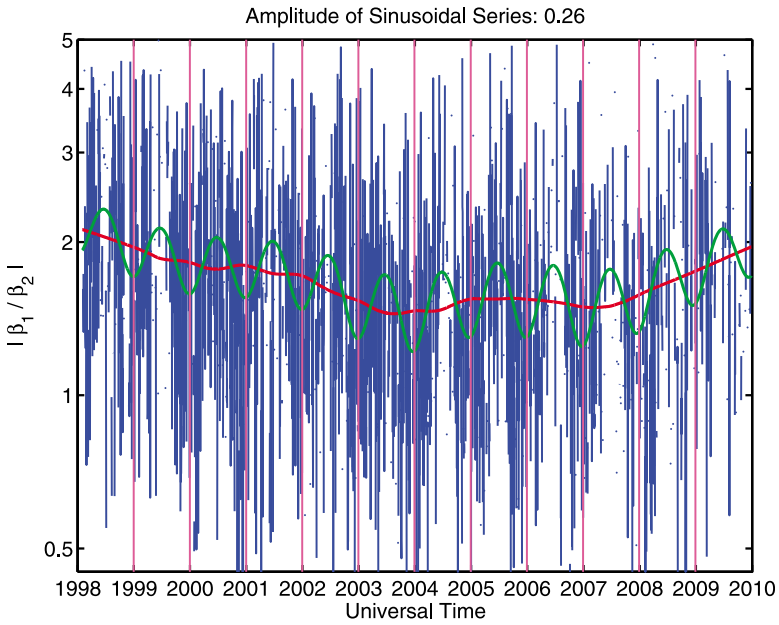

Figure 11. As for Figure 5 with sinusoidal annual component.

[24] Regarding the evidence of the semiannual peak, it is possible that some contributions arise because variations containing strong signals at frequency f but with a non-sinusoidal structure will contain power at higher-order harmonic components at frequencies $2f$, $3f$, etc [e.g., *Shumway and Stoffer*, 2006]. Thus, the peak at 6.2 months can be attributed partially to higher-order harmonic components of the 12.2 months peak. However, there may be physically important sources of the contribution at $2f$. It has long been recognized that geomagnetic activity follows a semiannual variation, with higher activity during equinox and weaker during solstice. Three theories have been proposed to explain the physical mechanism, the axial hypothesis [*Cortie*, 1912; *Bohlin*, 1977], the equinoctial hypothesis [*McIntosh*, 1959; *Svalgaard*, 1977], and the Russell-McPherron effect [*Russell and McPherron*, 1973]. It is not the purpose of this study to evaluate any of the above theories. A semiannual variation of *DUR* of the PC index is expected; our contribution is to have identified that the relative importance of the dominant currents that produce the PC magnetic signature varies systematically with solar cycle and also on shorter time scales.

[25] In order to quantify the mean amplitude of the annual variation, we use a first-order approximation through a regression analysis applied to the daily *DUR* time series with $R^2 \geq 0.5$ with predetermined frequency corresponding to the highest peak in Figure 10,

$$DUR = \text{trend} + A_1 \sin(2\pi t/365) + A_2 \cos(2\pi t/365) + \varepsilon_t, \quad (26)$$

where the trend is pre-fixed as the solar cycle trend calculated in section 3.1, A_1, A_2 are regression coefficients, and ε_t are residuals. The use of equation (26) is justified by the strength of the signal at a frequency corresponding to 1 year in Figure 10. The fit to the *DUR* obtained from equation (26) is shown in Figure 11, superposed on the daily variation from Figure 5. The ratio peaks in summer, which is consistent with our previous discussion. The magnitude, i.e., $A = (A_1^2+A_2^2)^{1/2}$, of the sinusoidal variation is $\pm$ 0.26. Thus, the summer-winter variation is estimated to be $\pm$ 15%.

4. Discussion and Conclusions

[26] In this study, we followed the analysis by Gao et al. (submitted manuscript, 2011) who decomposed the PC index into two primary components, a directly driven component proportional to the Kivelson-Ridley electric field ($E_{\text{K-R}}$) and an unloading component, linked to the auroral AL index and quantified as AL_U through a linear regression in equation (10). We applied the analysis on a daily basis from 1 February 1998 to 31 December 2009 to encompass solar cycle 23. Then we statistically studied the variation of driven and unloading contribution to the PC index by defining the driven-to-unloading ratio (*DUR*) (equation (16)) and analyzing its properties on different time scales. We found that the *DUR* varied systematically over solar cycle 23. As solar activity increases, the *DUR* decreases; when solar activity decays, the *DUR* increases.

[27] It is tempting to put forward possible explanations of the results of our statistical analysis. Here we provide suggestions that have not been fully tested but provide explanations of our results that we believe are plausible. We explain the nonintuitive finding regarding the change through the solar cycle of the relative contributions of a driven component and an unloading component in terms of a nonlinear relation between AL_U and $E_{\text{K-R}}$. We relate the latter quantities by the nonlinear form shown in equation (20), where both $\Sigma_{\text{E-P}}$ and $E_{\text{K-R}}$ are enhanced in a HSS. If $\Sigma_{\text{E-P}} \propto P_e^{1/2}$ as suggested by *Østgaard et al.* [2002], $\Sigma_{\text{E-P}}$ increases in association with stronger high-speed streams in the solar wind as solar activity approaches maximum and peaks slightly after the solar maximum [*Emery et al.*, 2009], causing a decrease in *DUR*. Then, *DUR* recovers following the decrease of P_e, or equivalently $\Sigma_{\text{E-P}}$.

[28] Strong annual variation of *DUR* is also identified and attributed to the differences in the dominant source of EUV conductance in the polar cap and in the auroral zone. The *DUR* peaks in summer and decreases in winter, because in summer the Hall conductance, Σ_H, caused by solar illumination is expected to increase as the solar zenith angle decreases [e.g., *Robinson and Vondrak*, 1984], and thus, stronger Hall currents are likely to be induced in summer, which results in stronger control of the PC index by the solar wind. The auroral zone conductance linked to electron precipitation also varies with season, but is likely to be less important in tuning the driven and unloading contributions to the PC index. Thus, due to higher Hall conductance resulting from enhanced solar illumination, a higher *DUR* in summer than in winter can be understood [*Robinson and Vondrak*, 1984; *Vennerstrøm et al.*, 1991].

[29] The driven, unloading processes are very complicated solar wind, magnetosphere-ionosphere coupling processes that are not likely to be fully described in terms of variations within a solar cycle and annual variations. As seen from Figure 11, only part of the variance of *DUR* can be understood as the sum of variations within a solar cycle and annual variations. We have not fully identified all the factors that contribute to *DUR* in controlling polar cap dynamics, but we believe that this statistical study of the polar cap response will provide a useful basis for future studies of polar cap dynamics.

[30] **Acknowledgments.** Y. Gao acknowledges support from NASA under grant NNX07AC93G. He appreciates having been given the opportunity to pursue this work during his graduate study at the department of Earth and Space Sciences in University of California, Los Angeles. He also appreciates R. L. McPherron and K. K. Khurana for helpful discussions. Y. Gao is grateful to B. Emery and an anonymous reviewer for their careful review and suggestive comments. The PCN index data were available from ftp://ftp.space.dtu.dk/WDC/indices/pcn. The PCS index data can be downloaded from http://www.aari.nw.ru. The AE index data are provided by http://wdc.kugi.kyoto-u.ac.jp. The ACE data are propagated by J. M. Weygand using the technique of *Weimer et al.* [2003] and are available through the Virtual Magnetospheric Observatory (VMO) (http://vmo.igpp.ucla.edu).

[31] Masaki Fujimoto thanks the reviewers for their assistance in evaluating this paper.

References

Akaike, H. (1973), Information theory and an extension of the maximum likelihood principle, paper presented at International Symposium on Information Theory, Tsahkadsor, Armenia.

Akasofu, S. I. (1979), What is a magnetospheric substorm?, in *Dynamics of Magnetosphere*, edited by S. I. Akasofu, pp. 447–460, D. Reidel, Dordrecht, Netherlands.

Ashour-Abdalla, M., R. J. Walker, V. Peroomian, and M. El-Alaoui (2008), On the importance of accurate solar wind measurements for studying magnetospheric dynamics, *J. Geophys. Res.*, *113*, A08204, doi:10.1029/2007JA012785.

Axford, W. I. (1964), Viscous interaction between the solar wind and the Earth's magnetosphere, *Planet. Space Sci.*, *12*, 45–53, doi:10.1016/0032-0633(64)90067-4.

Bargatze, L. F., D. N. Baker, E. W. Hones Jr., and R. L. McPherron (1985), Magnetospheric impulse response for many levels of geomagnetic activity, *J. Geophys. Res.*, *90*, 6387–6394, doi:10.1029/JA090iA07p06387.

Bohlin, J. D. (1977), Extreme-ultraviolet observations of coronal holes, *Sol. Phys.*, *51*, 377–398, doi:10.1007/BF00216373.

Borovsky, J. E., B. Lavraud, and M. M. Kuznetsova (2009), Polar cap potential saturation, dayside reconnection, and changes to the magnetosphere, *J. Geophys. Res.*, *114*, A03224, doi:10.1029/2009JA014058.

Chun, F. K., D. J. Knipp, M. G. McHarg, G. Lu, B. A. Emery, S. Vennerstrøm, and O. A. Troshichev (1999), Polar cap index as a proxy for hemispheric Joule heating, *Geophys. Res. Lett.*, *26*, 1101–1104, doi:10.1029/1999GL900196.

Chun, F. K., D. J. Knipp, M. G. McHarg, J. R. Lacey, G. Lu, and B. A. Emery (2002), Joule heating patterns as a function of polar cap index, *J. Geophys. Res.*, *107*(A7), 1119, doi:10.1029/2001JA000246.

Cleveland, W. S. (1979), Robust locally weighted regression and smoothing scatterplots, *J. Am. Stat. Assoc.*, *74*, 829–836, doi:10.2307/2286407.

Cortie, A. L. (1912), Sunspots and terrestrial magnetic phenomena, 1898–1911: The cause of the annual variation in magnetic disturbance, *Mon. Not. R. Astron. Soc.*, *73*, 52–60.

Emery, B. A., V. Coumans, D. S. Evans, G. A. Germany, M. S. Greer, E. Holeman, K. Kadinsky-Cade, F. J. Rich, and W. Xu (2008), Seasonal, Kp, solar wind, and solar flux variations in long-term single-pass satellite estimates of electron and ion auroral hemispheric power, *J. Geophys. Res.*, *113*, A06311, doi:10.1029/2007JA012866.

Emery, B. A., I. G. Richardson, D. S. Evans, and F. J. Rich (2009), Solar wind structure sources and periodicities of auroral electron power over three solar cycles, *J. Atmos. Terr. Phys.*, *71*, 1157–1175, doi:10.1016/j.jastp.2008.08.005.

Fiori, R. A. D., A. V. Koustov, D. Boteler, and R. A. Makarevich (2009), PCN magnetic index and average convection velocity in the polar cap inferred from SuperDARN radar measurements, *J. Geophys. Res.*, *114*, A07225, doi:10.1029/2008JA013964.

Hairston, M. R., R. A. Heelis, and F. J. Rich (1998), Analysis of the ionospheric cross polar cap potential drop using DMSP data during the National Space Weather Program study period, *J. Geophys. Res.*, *103*, 26,337–26,347, doi:10.1029/97JA03241.

Janzhura, A. S., and O. A. Troshichev (2008), Determination of the running quiet daily geomagnetic variation, *J. Atmos. Terr. Phys.*, *70*, 962–972, doi:10.1016/j.jastp.2007.11.004.

Kan, J. R., and L. C. Lee (1979), Energy coupling function and solar wind-magnetosphere dynamo, *Geophys. Res. Lett.*, *6*, 577–580, doi:10.1029/GL006i007p00577.

Kivelson, M. G., and A. J. Ridley (2008), Saturation of the polar cap potential: Inference from Alfvén wing arguments, *J. Geophys. Res.*, *113*, A05214, doi:10.1029/2007JA012302.

Liou, K., J. F. Carbary, P. T. Newell, C.-I. Meng, and O. Rasmussen (2003), Correlation of auroral power with the polar cap index, *J. Geophys. Res.*, *108*(A3), 1108, doi:10.1029/2002JA009556.

McComas, D. J., S. J. Bame, P. Barker, W. C. Feldman, J. L. Phillips, P. Riley, and J. W. Griffee (1998), Solar Wind Electron Proton Alpha Monitor (SWEPAM) for the Advanced Composition Explorer, *Space Sci. Rev.*, *86*, 563–612, doi:10.1023/A:1005040232597.

McIntosh, D. H. (1959), On the annual variation of magnetic disturbance, *Philos. Trans. R. Soc. London A*, *251*, 525–552, doi:10.1098/rsta.1959.0010.

McPherron, R. L., and D. N. Baker (1993), Factors influencing the intensity of magnetospheric substorms, *J. Atmos. Terr. Phys.*, *55*, 1091–1122, doi:10.1016/0021-9169(93)90040-6.

Myers, R. H. (2000), *Classical and Modern Regression with Applications* 2nd ed., 488 pp., Duxbury, Pacific Grove, Calif.

Østgaard, N., R. R. Vondrak, J. W. Gjerloev, and G. Germany (2002), A relation between the energy deposition by electron precipitation and geomagnetic indices during substorms, *J. Geophys. Res.*, *107*(A9), 1246, doi:10.1029/2001JA002003.

Ridley, A. J. (2000), Estimations of the uncertainty in timing the relationship between magnetospheric and solar wind processes, *J. Atmos. Terr. Phys.*, *62*, 757–771, doi:10.1016/S1364-6826(00)00057-2.

Ridley, A. J. (2007), Effects of seasonal changes in the ionospheric conductances on magnetospheric field-aligned currents, *Geophys. Res. Lett.*, *34*, L05101, doi:10.1029/2006GL028444.

Ridley, A. J., and E. A. Kihn (2004), Polar cap index comparisons with AMIE cross polar cap potential, electric field, and polar cap area, *Geophys. Res. Lett.*, *31*, L07801, doi:10.1029/2003GL019113.

Robinson, R. M., and R. R. Vondrak (1984), Measurements of E region ionization and conductivity produced by solar illumination at high latitudes, *J. Geophys. Res.*, *89*, 3951–3956, doi:10.1029/JA089iA06p03951.

Ruohoniemi, J. M., and K. B. Baker (1998), Large-scale imaging of high-latitude convection with Super Dual Auroral Radar Network HF radar observations, *J. Geophys. Res.*, *103*, 20,797–20,811, doi:10.1029/98JA01288.

Russell, C. T., and R. L. McPherron (1973), Semiannual variation of geomagnetic activity, *J. Geophys. Res.*, *78*, 92–108, doi:10.1029/JA078i001p00092.

Shumway, R. H., and D. S. Stoffer (2006), *Time Series Analysis and Its Applications: With R Examples*, 2nd ed., 575 pp., Springer, New York.

Siscoe, G. L., G. M. Erickson, B. U. Ö. Sonnerup, N. C. Maynard, J. A. Schoendorf, K. D. Siebert, D. R. Weimer, W. W. White, and G. R. Wilson (2002), Hill model of transpolar potential saturation: Comparisons with MHD simulations, *J. Geophys. Res.*, *107*(A6), 1075, doi:10.1029/2001JA000109.

Siscoe, G. L., J. Raeder, and A. J. Ridley (2004), Transpolar potential saturation models compared, *J. Geophys. Res.*, *109*, A09203, doi:10.1029/2003JA010318.

Smith, C. W., J. L'Heureux, N. F. Ness, M. H. Acuña, L. F. Burlaga, and J. Scheifele (1998), The ACE magnetic fields experiment, *Space Sci. Rev.*, *86*, 613–632, doi:10.1023/A:1005092216668.

Spiro, R. W., P. H. Reiff, and L. J. Maher Jr. (1982), Precipitating electron energy flux and auroral zone conductances—An empirical model, *J. Geophys. Res.*, *87*, 8215–8227, doi:10.1029/JA087iA10p08215.

Stauning, P. (2011), Comment on "The PC index: Review of methods", by McCreadie and Menvielle (2010), *Ann. Geophys.*, *29*, 1137–1146, doi:10.5194/angeo-29-1137-2011.

Svalgaard, L. (1977), Geomagnetic activity: Dependence on solar wind parameters, in *Coronal Holes and High Speed Wind Streams*, edited by J. B. Zirker, 371 pp., Colo. Assoc. Univ. Press, Boulder.

Takalo, J., and J. Timonen (1998), Comparison of the dynamics of the AU and PC indices, *Geophys. Res. Lett.*, *25*, 2101–2104, doi:10.1029/98GL01614.

Troshichev, O. A., and R. Y. Lukianova (2002), Relation of PC index to the solar wind parameters and substorm activity in time of magnetic storms, *J. Atmos. Terr. Phys.*, *64*, 585–591, doi:10.1016/S1364-6826(02)00016-0.

Troshichev, O. A., V. G. Andrezen, S. Vennerstrøm, and E. Friis-Christensen (1988), Magnetic activity in the polar cap—A new index, *Planet. Space Sci.*, *36*, 1095–1102, doi:10.1016/0032-0633(88)90063-3.

Troshichev, O. A., H. Hayakawa, A. Matsuoka, T. Mukai, and K. Tsuruda (1996), Cross polar cap diameter and voltage as a function of *PC* index and interplanetary quantities, *J. Geophys. Res.*, *101*, 13,429–13,435, doi:10.1029/95JA03672.

Troshichev, O. A., R. Y. Lukianova, V. O. Papitashvili, F. J. Rich, and O. Rasmussen (2000), Polar cap index (PC) as a proxy for ionospheric electric field in the near-pole region, *Geophys. Res. Lett.*, *27*, 3809–3812, doi:10.1029/2000GL003756.

Troshichev, O. A., A. Janzhura, and P. Stauning (2006), Unified PCN and PCS indices: Method of calculation, physical sense, and dependence on the IMF azimuthal and northward components, *J. Geophys. Res.*, *111*, A05208, doi:10.1029/2005JA011402.

Vennerstrøm, S. (1991), The geomagnetic activity index PC, PhD dissertation, 105 pp., Dan. Meteorol. Inst., Copenhegan.

Vennerstrøm, S., E. Friis-Christensen, O. A. Troshichev, and V. G. Andresen (1991), Comparison between the polar cap index, PC, and the auroral electrojet indices AE, AL, and AU, *J. Geophys. Res.*, *96*, 101–113, doi:10.1029/90JA01975.

Walker, G. (1931), On periodicity in series of related terms, *Proc. R. Soc. London, Ser. A*, *131*, 518–532, doi:10.1098/rspa.1931.0069.

Weimer, D. R., D. M. Ober, N. C. Maynard, M. R. Collier, D. J. McComas, N. F. Ness, C. W. Smith, and J. Watermann (2003), Predicting interplanetary magnetic field (IMF) propagation delay times using the minimum variance technique, *J. Geophys. Res.*, *108*(A1), 1026, doi:10.1029/2002JA009405.

Yule, G. U. (1927), On a method of investigating periodicities in disturbed series, with special reference to Wolfer's sunspot numbers, *Philos. Trans. R. Soc. London A*, *226*, 267–298, doi:10.1098/rsta.1927.0007.

Y. Gao, M. G. Kivelson, and R. J. Walker, Department of Earth and Space Sciences, University of California, 595 Charles Young Dr. E., Los Angeles, CA 90095-1567, USA. (ygao@igpp.ucla.edu)

J. M. Weygand, Institute of Geophysics and Planetary Physics, University of California, 3845 Slichter Hall, PO Box 951567, Los Angeles, CA 90095-1567, USA.